# Modified ZnSe nanoparticles for removal of heavy metal iron (Fe) from aqueous solution

Khurshed A. Shah<sup>1</sup>, Humaira S. Wani<sup>2</sup>, S. M. A. Andrabi<sup>2</sup>, Quinton L. Williams<sup>3</sup>

- <sup>1</sup>PG Department of Physics, Sri Pratap College, Cluster University Srinagar, J&K-190001, India
- <sup>2</sup>Department of Applied Sciences, Institute of Technology, Zakura Campus, University of Kashmir, Srinagar, J&K-190006, India

Corresponding author: Khurshed A. Shah, drkhursheda@gmail.com

ABSTRACT Iron is a heavy metal found in water due to natural geological sources, household trash, industrial waste, and numerous by-products. An excessive amount of iron in drinking water can lead to significant health issues in humans. In the current study, metallic Zn–Se NPs modified with Ag and urea were synthesised via the sol-gel method and characterised by XRD, FESEM, EDX and FTIR. The synthesised ZnSe:Ag:Urea nanoparticles were used for the adsorptive removal of iron, a heavy metal, from water. Herein, we have utilised adsorption technology to extract iron ions from water, considering the toxicity of iron at high concentrations. Experimental batch adsorption studies were conducted on an aqueous solution containing Fe (III) ions under various conditions, including temperature, contact time, adsorbent dosage, and initial metal ion concentration. Results showed that iron adsorption was favourable, with a maximum removal percentage of 89.5 % under optimal room temperature conditions, optimal adsorbent dosage, and initial metal ion concentration. of 0.1 g/L and 100 mL, respectively. The iron absorption also reached an equilibrium state within 80 minutes of contact time by using ZnSe:Ag:Urea as the adsorbent.

KEYWORDS ZnSe nanoparticles, iron, heavy metal, absorption

ACKNOWLEDGEMENTS This work was supported by the JKST&IC-funded project (Grant No. JKST&IC/SRE/1172-74), CSIR-HRDG funded project (scheme no. 1510/23/EMR-II) and SERB (Grant No. CRG2022/006428-G)).

FOR CITATION Shah K.A., Wani H.S., Andrabi S.M.A., Williams Q.L. Modified ZnSe nanoparticles for removal of heavy metal iron (Fe) from aqueous solution. *Nanosystems: Phys. Chem. Math.*, 2025, **16** (5), 681–692.

# 1. Introduction

Clean water is one of the essential requirements for the existence of life on Earth. However, in recent years, the contamination of water has become a significant problem all around the globe. This is mainly because of industrialisation and huge population growth spurred by expanding urbanisation, leading to an increase in contamination of water at an alarming rate [1,2]. Heavy metals, the major water pollutant, pose the most significant damage to human health and the environment as they are highly poisonous, even at low concentrations. This non-biodegradable material accumulates through the food chain and destroys aquatic life while posing significant risks to human health [3]. There is a substantial increase in water pollution due to heavy metals because of the continuous increase in urban and rural industrial and agricultural activities such as the preservation of wood and dyes, electroplating, steel production, industrial smelting, sewage irrigation, textiles, fertilisers, battery manufacturing, construction, pharmaceutical, metallurgical industries, etc. [4]. Heavy metals like Hg, Cr, As, Zn, Ni, and Cd are highly hazardous to human beings, and exposure to even small amounts of these heavy metals cause severe damage to human health [5]. These metals naturally infiltrate water bodies as rainwater seeps through rocks, resulting in the dissolution of trace amounts of metals into the water. This water subsequently flows into larger water bodies, which are utilized by individuals for various purposes. Iron is one of the metals that is naturally present in water. It is the fourth most abundant element on the planet, and it holds the second position in terms of abundance within the earth's crust [6]. It is present in significant amounts within rocks and soil systems globally. This mineral nutrient is essential, contributing to the regulation of energy metabolism. Moreover, it serves as a crucial component in hemoglobin, myoglobin, and various enzymes. Insufficient iron levels in the body can lead to iron deficiency, anemia, fatigue, and a heightened vulnerability to various infections [7]. Water bodies obtain iron from either natural geological sources or through the disposal of household waste and industrial discharges [8]. The primary sources of iron in surface water include pollution originating from the iron and steel industries, as well as mining activities and the corrosion of metals [9]. In addition to surface water, iron is found in groundwater as well. The primary cause of iron's presence in groundwater

<sup>&</sup>lt;sup>3</sup>Department of Physics and Astronomy, Howard University, NW, Washington, DC 20059, USA

is the leaching process from iron-rich rocks and minerals [10]. The levels of iron found in both surface and groundwater range from 3 to 4 mg/L up to 15 mg/L [11]. The concentration of iron in the groundwater of West Bengal, India, ranges from 2 to 10 mg/L [12]. In the Ganga river, near the Fazalpur industrial area located in the Moradabad district of Uttar Pradesh, India, iron concentrations have been recorded as high as 6 mg/L [13]. Furthermore, the groundwater in Assam, an eastern state of India, exhibits significant contamination with high levels of iron [14-16]. It is important to note that the permissible limit for iron in drinking water is set at 0.3 mg/L [17,18]. While initial concentrations exceeding this limit may not pose immediate health risks, prolonged consumption of water with elevated iron levels can lead to a condition known as iron overload [19]. Excessive consumption of iron can result in the disruption of hematopoiesis by harming both the progenitor cells and the supportive microenvironment necessary for this process. If iron overload is not addressed, it may progress to hemochromatosis, which can cause damage to various organs in the body [20-25]. The initial manifestations consist of weight reduction, joint discomfort, and exhaustion. Additionally, ocular conditions like retinitis, conjunctivitis, and choroiditis, along with cancer and cardiovascular diseases, represent some of the prevalent health challenges associated with elevated levels of iron in the water [26]. In addition to the aforementioned health-related concerns, various other issues associated with elevated iron levels in water have been documented. At higher concentrations, this metal contributes to an unpleasant odor, a metallic flavor, and a reddish hue in the water [27]. It also leads to the formation of stains and streaks on laundry and plumbing fixtures. The accumulation of softeners and pipelines caused by the precipitation of iron can result in unfavorable conditions within the water distribution systems [28]. Elevated levels of iron can serve as a substrate for specific bacterial species. The interior surfaces of pipes provide an optimal environment for these bacteria. Their populations can grow to such an extent that they begin to obstruct pipes, thereby diminishing the water flow rate within the pipeline. Once these bacterial colonies become established, their removal from the pipeline poses significant challenges. Additionally, pipelines constructed from iron frequently encounter issues such as punctures and leaks, as noted in references [28,29]. The decomposition of these bacteria results in the generation of foul odors and undesirable tastes in the water supply [28]. This calls for the effective treatment of water in order to remove the elevated levels of iron and produce safe and clean water. A number of methods have been reported in the past for such purpose.

In the present study, ZnSe nanoparticles doped with Ag and functionalized with urea (denoted ZnSe:Ag:Urea) were synthesized via the sol-gel method and comprehensively characterized by X-ray diffraction (XRD), field emission scanning electron microscopy (FESEM), energy-dispersive X-ray spectroscopy (EDX), and Fourier transform infrared spectroscopy (FTIR). Set experiments were conducted to investigate the adsorptive removal of Fe(III) under varying conditions of temperature, contact time, adsorbent dosage, and initial ion concentration. The synthesized ZnSe:Ag:Urea nanoparticles demonstrated a maximum iron removal efficiency of 89.5 % at optimal conditions – an adsorbent dosage of 0.1 g/L, solution volume of 100 mL, room temperature, and equilibrium achieved within 80 minutes.

This work aims to (i) validate the synthesis and modification strategy for ZnSe:Ag:Urea nanoparticles; (ii) Assess their potential as an efficient and regenerable nano-adsorbent for water treatment applications.

## 2. Experimental details

# 2.1. Materials

Zinc acetate dihydrate  $(Zn(CH_3CO_2)_2 \cdot 2H_2O)$ , selenium powder, Silver nitrate  $(AgNO_3)$ , urea  $(NH_2CONH_2)$ , hydrazine hydrate  $(N_2H_6)$ , ethylene glycol  $(OHCH_2CH_2OH)$  and methanol were used in this study. All chemicals, purchased from Merck, India, were used as received and without further purification and were of analytical reagent grade (>95% purity).

## 2.2. Methodology

Urea and silver modified ZnSe nanoparticles were synthesised by a chemical route called the sol-gel method. In a typical reaction, 0.5 M zinc acetate solution was prepared by dissolving 1.317 g of zinc acetate dehydrate salt in 12 mL of methanol, whereas that of selenium(1 M) was prepared by dissolving 0.631 g of selenium in 8 mL of methanol. The two solutions were sonicated for 30 minutes in an ultrasonic bath, transferred to a 200 mL beaker, and again sonicated for 30 minutes. Next, the prepared solution was refluxed at 80 °C on a hot plate magnetic stirrer for 3 hours. After the first 10 minutes,10 ml hydrazine hydrate, a reducing agent, and 15 ml ethylene glycol, a stabilising agent, were added dropwise to the solution. Then, the solution was doped with 50 % silver nitrate and 50 % urea. After about 40 minutes, the reaction was completed (i.e., the solution was converted into gel) and stirring was stopped. The gel that formed was kept at a temperature of 80 °C to allow the volatile impurities to escape, and a dark-grey coloured xerogel was formed, which was then washed with deionised water 3-4 times using a centrifuge at a speed of 6000 rpm. Finally, the resultant product was dried in an oven at 70 °C for 24 hours and yielded a dry mass which was crushed in a mortar and pestle to reduce particle sizes to the nanoscale. Fig. 1. illustrates the detailed Experimental procedure for synthesising the Urea:Ag:ZnSe nanoparticles.

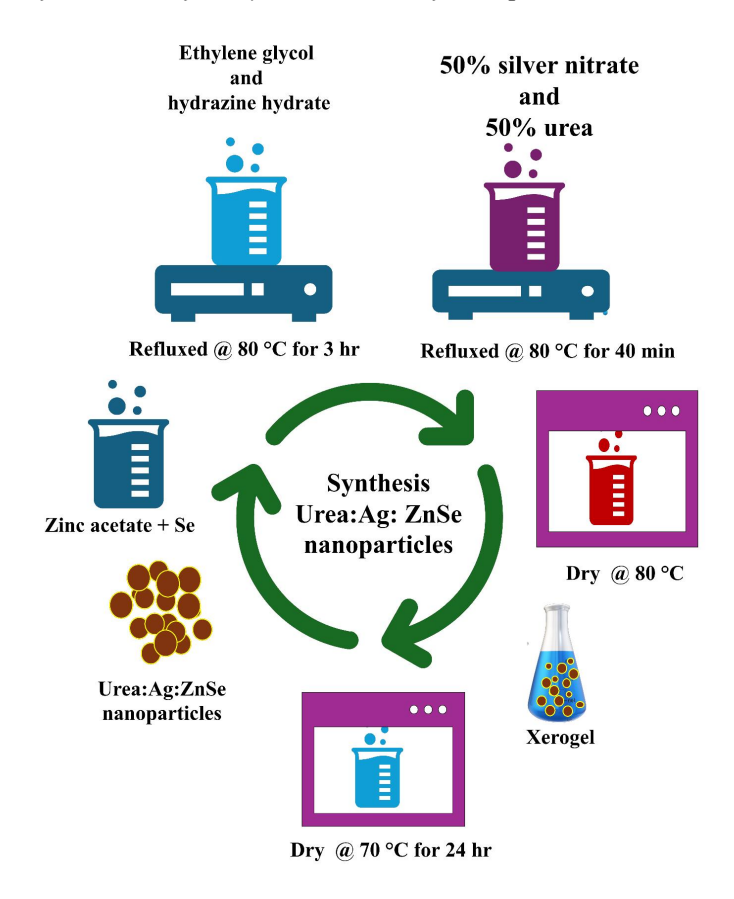


FIG. 1. Experimental procedure for the synthesis of the Urea:Ag:ZnSe nanoparticles

# 3. Results and discussion

### 3.1. Characterization of Urea: Ag: ZnSe nanoparticles

The synthesised ZnSe nanoparticles were characterised using X-ray diffraction (XRD), Field Emission Scanning Electron Microscopy (FE-SEM), Fourier Transform Infrared Spectroscopy (FTIR), Energy Dispersive X-Ray (EDX), Particle Analyzer and Zeta Potential studies. The crystal structure of the sample ZnSe NPs was investigated by XRD using Smart Lab 3kW X-ray Diffractometer from Rigaku operating at a voltage 40 kV and filament current 30 mA with CuK $\beta$  radiation( $\lambda = 1.392$  Å) and scanning rate of 5.0985 deg/min and scan range set from 20° to 80°.The FE-SEM (Gemini SEM 500 from Carl Zeiss) and ultra dry Compact EDS Detector (Thermo Scientific<sup>TM</sup>) are used for high-resolution imaging and elemental analysis. Energy Dispersive X-Ray Spectra (EDS) was used to identify samples' elemental composition and purity by atom percentage of metal, and FE-SEM examination confirmed the surface shape of ZnSe NPs. The phase composition and molecular structure analysis were done using FTIR (Shimadzu). A lithium tantalate detector, a Perkin Elmer Spectrum 2 (USA), was used to obtain Fourier-Transform Infrared Spectra in the 400 – 4000 cm<sup>-1</sup> range. With a resolution of 4 cm<sup>-1</sup>, a single scan produced the spectra to identify and characterise functional groups.

- 3.1.1. XRD analysis. Powder X-ray diffraction (XRD) investigations were conducted on Ag and urea-doped ZnSe NPs. CuK $\beta$  radiation of wavelength 1.392 Å and scanning rate of 5.0985 deg/min). The XRD profile (Fig. 2) reveals the presence of zinc selenide (ZnSe), silver selenide (Ag<sub>2</sub>Se), Urea (NH<sub>2</sub>CONH<sub>2</sub>) and selenium (Se) in the as-prepared nanoparticles. The peak at  $2\theta = 27.2^{\circ}$  (111),  $45.22^{\circ}$  (220),  $53.58^{\circ}$  (311),  $67.31^{\circ}$  (400) and  $72.68^{\circ}$  (203) corresponds to ZnSe [30–37]. The peak at  $2\theta = 33.4^{\circ}$  (112),  $34.68^{\circ}$  (121),  $39.94^{\circ}$  (103) and  $40.268^{\circ}$  (122) correspond to Ag<sub>2</sub>Se [38, 39]. Two peaks of NH<sub>2</sub>CONH<sub>2</sub> (urea) have been obtained at  $2\theta = 22.76^{\circ}$  and  $36.92^{\circ}$  due to diffraction from (110) and (210) planes, respectively [40,41]. A single diffraction peak for by-product Se has also been obtained. Also the peak corresponding to Ag obtained at  $2\theta = 37^{\circ}$  (111),  $46^{\circ}$  (200),  $64^{\circ}$  (220), and  $78^{\circ}$  (311) [42]. The average crystallite size has been estimated using Scherrer's formula:  $G = (0.9\lambda)/(\beta \cos \theta)$ , where  $\lambda$  is the wavelength of CuK $\alpha$  radiation ( $\lambda = 1.541$  Å),  $\beta$  is the full width at half maximum (FWHW) of the intensity of the corresponding peak and  $\theta$  is half the angle between the incident and the scattered X-ray beams. The average particle size of ZnSe:Ag:Urea NPs was calculated to be 19.911 nm.
- 3.1.2. Morphological studies by FE-SEM. The surface morphology of urea and silver-modified zinc selenide nanoparticles was studied using an FE-SEM. The FE-SEM images (Fig. 3(a,b,c,d)) show that the synthetic Urea:Ag:Zn:Se nanoparticles are almost spherical and round-shaped with porous surfaces. Surface modification by silver and urea of ZnSe NPs

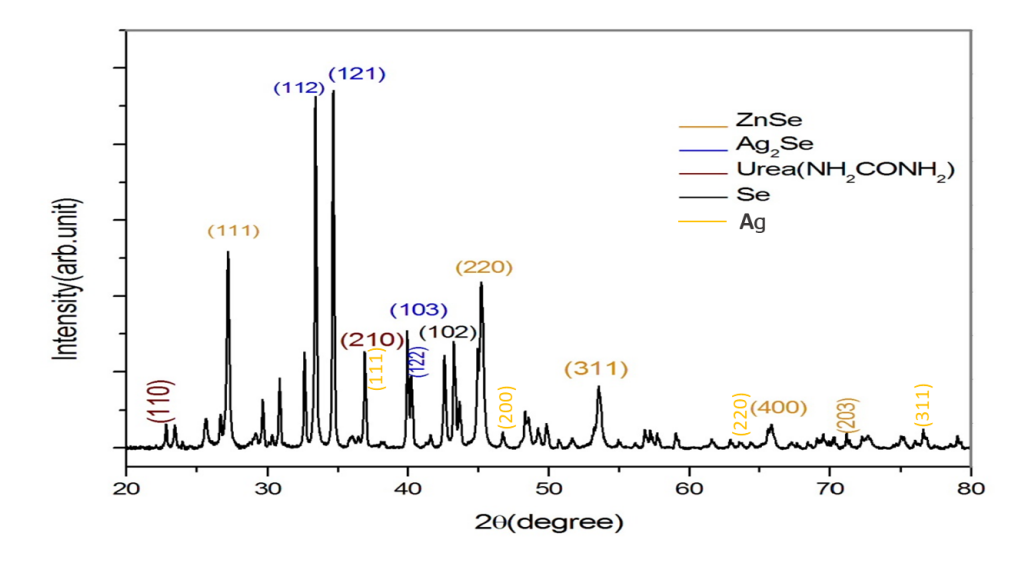


FIG. 2. XRD spectra of Urea and Ag doped ZnSe nanoparticles

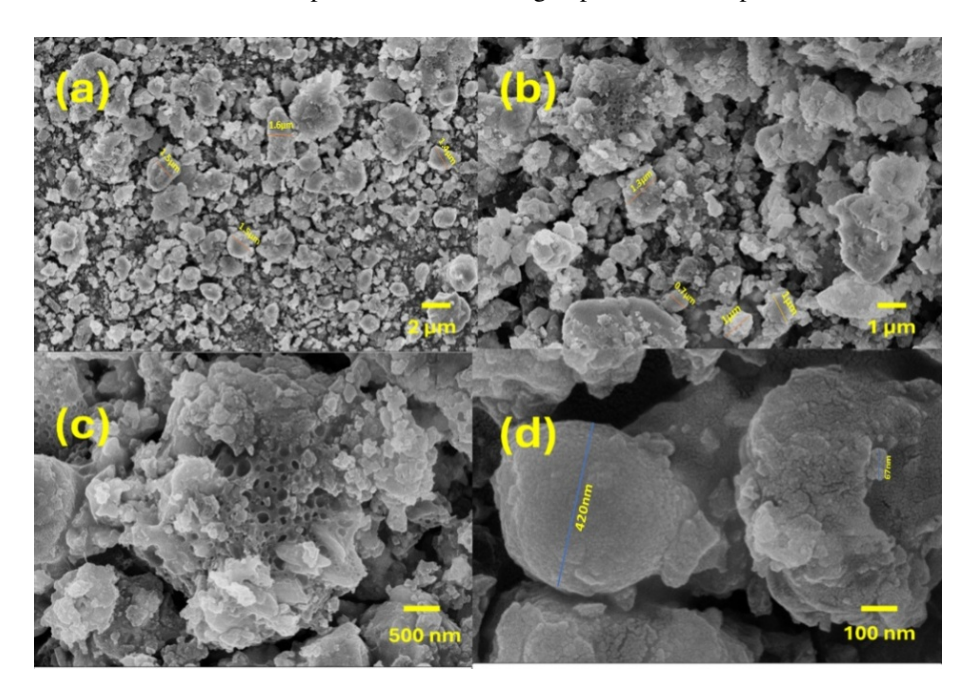


FIG. 3. FESEM images (a,b,c and d) of urea: Ag:Zn:Se nanoparticles for various magnifications

forms the porous structure. The material, as synthesised, consisted of highly facetted nanoparticles that were connected and clustered together.

- 3.1.3. Elemental composition analysis by EDX. The elemental composition of synthesised Urea:Ag:Zn:Se NPs was determined by Energy Dispersive X-Ray (EDX) spectroscopy. In the EDX spectra displayed in Fig. 4(a), 11 peaks could be seen for the parent material of urea:Ag:Zn:Se nanoparticles: three peaks for elemental zinc, three for selenium, two for silver and three for elements carbon, oxygen and nitrogen present in urea. Other small peaks in the spectrum indicate the presence of minor levels of Au, which are attributed to the coating procedure that the samples were subjected to preceding the EDX examination analysis confirms the presence of Zn (9.6 %), Se(19.7 %), Ag(16.2 %), urea (29.3 % C, 15.2 % N, 10.2 % O) as shown in Fig. 3(b).
- 3.1.4. Analysis of FTIR spectra. A view of the pure urea FTIR spectrum is presented in Fig. 5(a). The C=O stretching frequency is visible at 1677 cm<sup>-1</sup>. Stretching and deformation frequencies for N–H are observed at 3455 and 1625 cm<sup>-1</sup>, respectively. The C–N stretching frequency is visible at 1453 cm<sup>-1</sup> [43]. The FTIR spectra of pure ZnSe nanoparticles are depicted in Fig. 4(b). ZnSe vibrations are characterised by distinctive peaks at 480, 552, 612, 664, and 960 cm<sup>-1</sup>. The trace amount of  $H_2O$  in the solution explains the peak at 3204 cm<sup>-1</sup>, which was attributed to O–H stretching. Additionally,

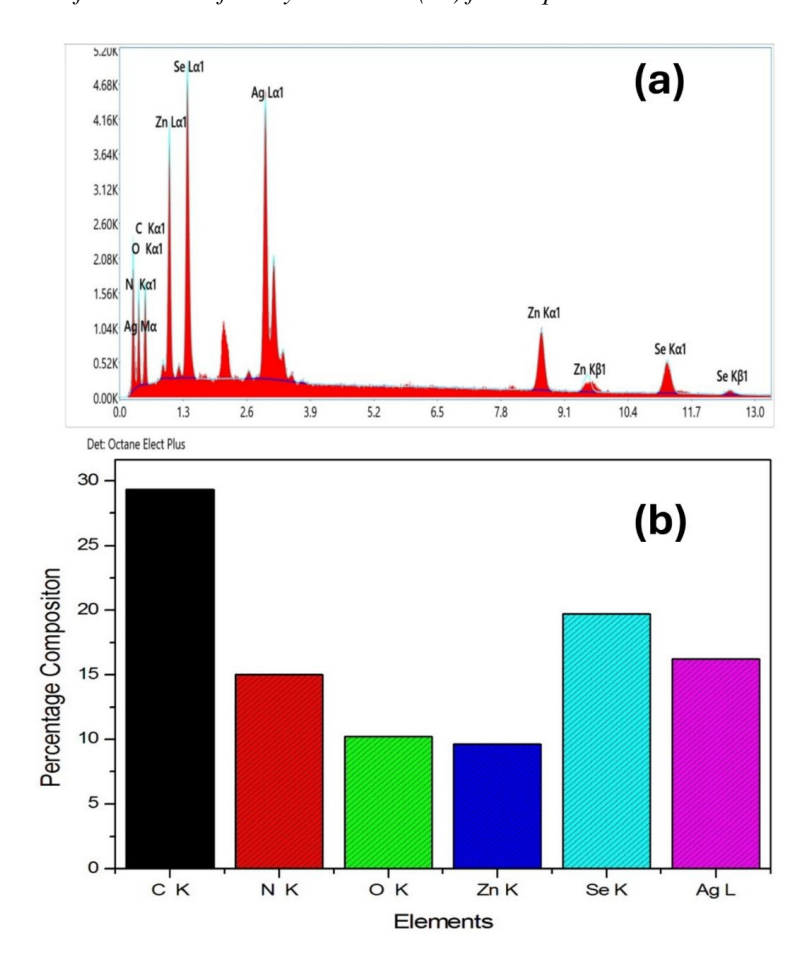


FIG. 4. (a) EDX spectrum;(b) The percentage elemental composition of urea: Ag:Zn:Se nanoparticles

the characteristic ZnSe absorption peak is represented by the peak at 960 cm $^{-1}$ , while the Se–O stretching bond causes the peak at 1134 cm $^{-1}$ . The peak at 3199 cm $^{-1}$  corresponds to the N–H stretching vibration band, indicating N<sub>2</sub>H<sub>4</sub>'s interaction with the zinc ion [44].

On the other hand, the FTIR spectra of ZnSe nanoparticles modified with silver and urea, as displayed in Fig. 5(c), show deviated and different numbers of peaks from those of pure ZnSe and pure urea, which suggests that new bonds are formed. ZnSe vibrations characterised by distinctive peaks 480, 550, 610 and 664 cm<sup>-1</sup> are shifted to 546, 620, 721 and 815 cm<sup>-1</sup>. The characteristic ZnSe absorption peak at 960 cm<sup>-1</sup> is shifted to 1051 cm<sup>-1</sup> while the peak at  $1134 \, \text{cm}^{-1}$ , caused by the Se–O stretching bond, is shifted to  $1150 \, \text{cm}^{-1}$ . This suggests an Ag–Se bond formation, which is also supported by XRD studies as  $Ag_2Se$  peaks are observed in XRD spectra. The kind and nature of the metal appear to impact how urea coordinates with metal ions. While Zn(II) coordinates to the oxygen of urea, Ag(II) preferentially coordinates to the nitrogen. If a nitrogen-to-metal connection exists in urea-metal complexes, the complex's vibrational spectrum differs greatly from that of the free urea molecule. The C=O (C=O)) would be adjusted to a higher frequency at roughly  $1700 \, \text{cm}^{-1}$ , and the N–H stretching frequencies would be shifted to lower values [45–48].

Here, in the FTIR spectra of synthesised Urea:Ag:Zn:Se NPs as shown in Fig. 4(c), the C=O stretching frequency 1677 cm<sup>-1</sup> of pure urea is shifted to 1701 cm<sup>-1</sup>. The C-N stretching frequency has shifted from 1453 to 1480 cm<sup>-1</sup>. However, the nitrogen-hydrogen bond stretching vibration peaks provide the best infrared signal for nitrogen. Two of these are seen in Fig. 4(c) at 3257 and 3142 cm<sup>-1</sup>, indicating the shift of the N-H stretching frequency to 3455 cm<sup>-1</sup> from that of pure urea. Also, hydrogen bonding is the reason for these peaks' reduced amplitudes but broader bases. It should be noted that the N-H stretching peaks are smaller and narrower than the O-H stretching peaks, which are broad and strong, although the O-H stretching peaks of functional groups such as alcohols and carboxylic acids also fall within this range (3500 to 3100 cm<sup>-1</sup>). Note that the O-H stretching peaks of functional groups like alcohols and carboxylic acids also fall in this range (3500 to 3100 cm<sup>-1</sup>), but these peaks are broad and strong compared to N-H stretching peaks, which are narrower and smaller. The N-H deformation frequency is visible at 1630 cm<sup>-1</sup>. This suggests urea has coordinated to the metal (Ag) through nitrogen. Further, the peaks at around 2887 and 2826 cm<sup>-1</sup> can be attributed to C-H stretching of urea. Thus, the FTIR study leads to the conclusion that Ag bridges the bond formation between ZnSe NPs and urea's Ag forms the bond with Se of ZnSe NPs, and nitrogen of NH<sub>2</sub> group of urea leads to the deviation of FTIR spectra of synthesised nanomaterial from that of pure urea and pure ZnSe NPs, respectively.

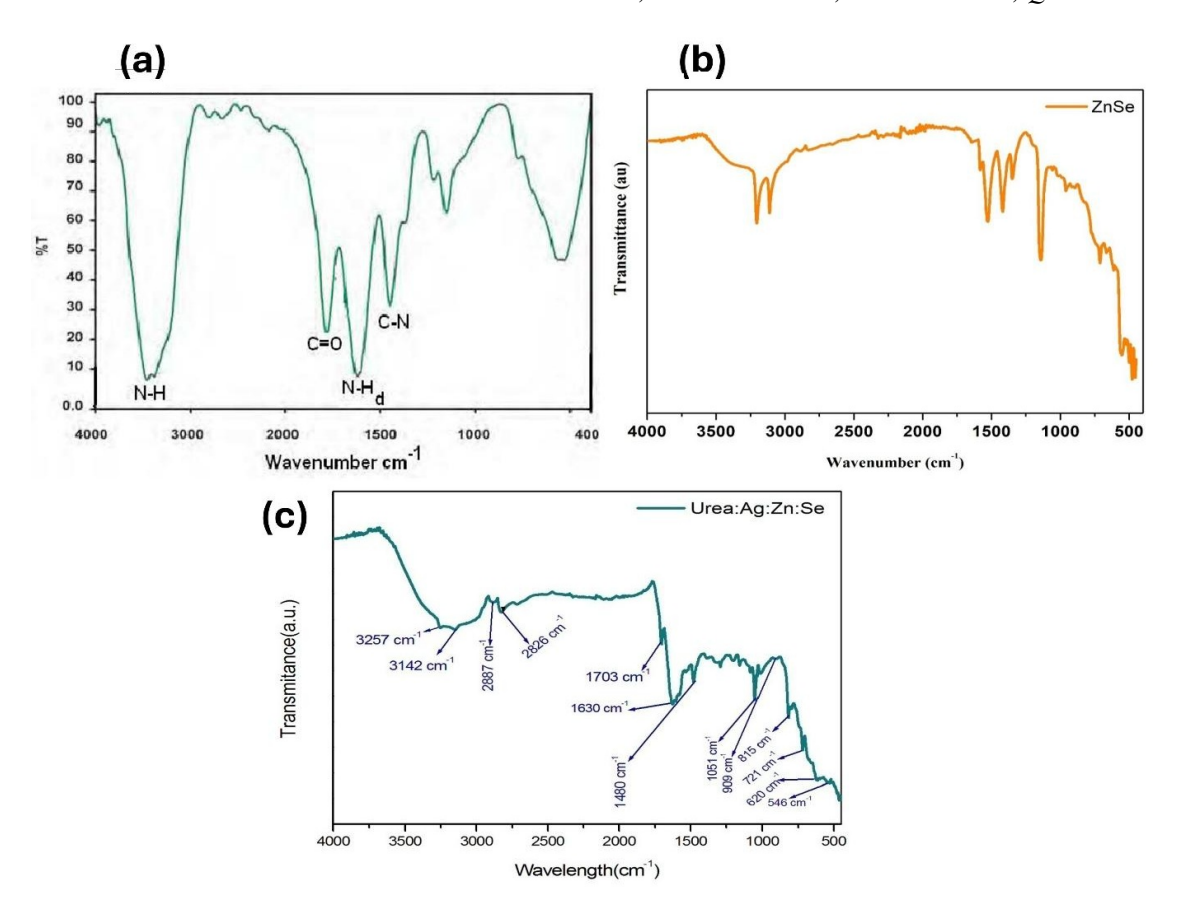


FIG. 5. FTIR spectra of (a) pure urea, (b) pure ZnSe NPs and synthesised Urea: Ag: Zn: Se NPs

## 4. Adsorption experiments

Batch adsorption experiments were conducted to determine how different parameters (initial conc of metal ion, amount of adsorbent, contact time and temperature) affected the removal rate of Fe and adsorption capacity of Ag and Urea modified ZnSe nanomaterial. Fe removal experiments were performed using 100 mL Erlenmeyer flasks containing 50 mL metal solution of desired concentration and specific amounts of adsorbent. An electric orbital shaker was used to shake the Erlenmeyer flasks at 200 rpm continuously. After the elapsed time, each flask's solution was filtered using Whatman filter paper, and the concentration of iron ions was determined using AAS(atomic absorption spectrophotometer). The ideal contact time was calculated at room temperature with 0.1 g/L of adsorbent and 100 mg/L of Fe. The 0.01 – 0.4 g/L and 5 – 250 mg/L, respectively, were used to study the effects of adsorbent dose and initial Fe concentration. At 25, 50, and 80 °C, the impact of solution temperature (25, 50, and 80 °C) on the effectiveness of Fe removal was examined. The amount of Fe adsorbed onto the adsorbent at each contact time ( $q_e$ ) was calculated using the eq. (1):

$$q_e = (C_0 - C_e) \cdot \frac{V}{m},\tag{1}$$

where  $C_0$  and  $C_e$  are initial and equilibrium concentration of Fe (mg/L), respectively. V is the volume of the aqueous phase (L) and m is the mass of adsorbent (ZnSe:Ag:Urea). The removal percentage of Fe was calculated using the following eq. (2):

Removal efficiency (%) = 
$$\frac{C_0 - C_i}{C_0} \cdot 100 \%$$
. (2)

#### 4.1. Effect of contact time

Figure 6 shows the effect of time on the Fe adsorption with an adsorbent dosage of 0.1 g and an initial Fe concentration = 100 mg/L/L. The removal rate increased significantly within the first 70 minutes, then increased marginally, reaching its steady state within 80 minutes. The availability of many empty active sites on the adsorbent surface may cause a substantial increase in adsorption efficiency. However, extending the duration of contact reduces the availability of iron ions to the adsorbent surface's active sites, decreasing the removal efficacy [49]. In other words, the reason for the constant value throughout the equilibrium phase is that heavy metal ions entirely occupy the vacant space. As time passes, no more adsorbent sites are available for the heavy metal ions to bind to [50]. Thus, the 90-minute contact period has been chosen as the ideal contact time for subsequent study.

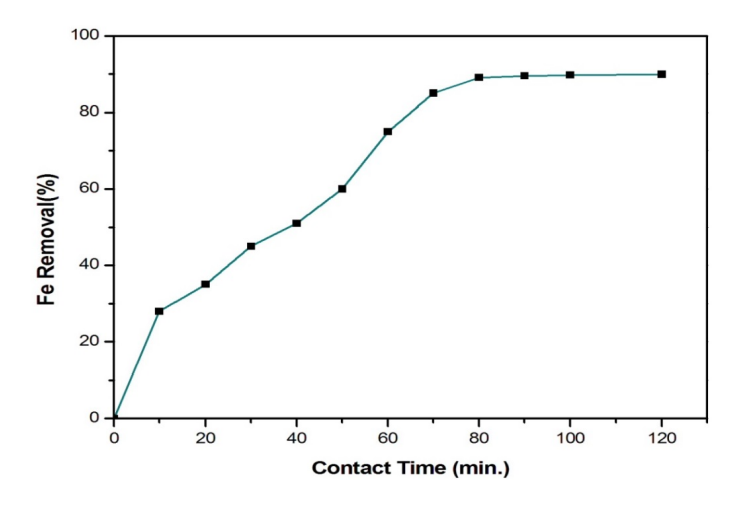


FIG. 6. Effect of contact time on the percentage removal of iron ions (adsorbentdosage, 0.1 g; initial Fe conc. = 100 mg/L; 200 rpm agitation speed; room temperature)

#### 4.2. Effect of initial metal (Fe) concentration

It was observed initially as the metal ion (Fe) concentration. Increases from 0-100 mg/L, the percentage of Fe removal increased from 46 to 89.6 %, which can be attributed to the higher number of available vacant sites on the adsorbent and the rise in the concentration gradient between the Fe ions in the solution and the Fe ions on the surface of the adsorbent [51]. Then, by further increasing the initial Fe ion concentration from 100-250 mg/L, the Fe removal percentage decreased from 89.6 to 73.46 %. This is because with the progress of the adsorption process, the available vacant sites of the adsorbent reduce [52] and the concentration. The gradient of metal ions also decreases, leading to a decrease in iron removal percentage, eventually leading to equilibrium. Table 1 shows the impact of different Fe concentrations (5, 10, 50, 100, 150, and 250 mg/L) on the percentage removal of iron, the same is plotted in Fig. 7.

Initial Fe conc. $(mg/L)$ $C_0$	Eq. Fe conc. $(mg/L)$ $C_e$	Fe Removal (%) $[(C_0 - C_e)/C_0] \cdot 100$	Eq. Adsorption Capacity (mg/g) $q_e = [(C_0 - C_e) \cdot V]/m$
5	2.7	46 %	1150
10	4.59	45.9 %	2705
50	13.9	72.2 %	18050
100	10.4	89.6 %	44800
150	24.6	83.6 %	62700
250	66.35	73.46 %	91825

TABLE 1. Adsorption data for Fe removal

# 4.3. Effect of adsorbent dosage

The experiment employed several adsorbent concentrations (0.01, 0.05, 0.1, 0.2, 0.3, and 0.4 g), with an initial concentration of 100 mg/L of Fe metal and a 90-minute contact duration.

As shown in Fig. 8, it is clear that initially, as the adsorbent dosage increases from 0.01 to 0.2 g, the removal percentage of Fe was enhanced from 42.34 to 85.76 % for 100 mg/L of Fe. This is because the availability of active sites on adsorbent increases, and hence there is a rise in the adsorption of Fe ions. Further, as the adsorbent dosage increases from 0.01 to 0.1 g, the rate of increase in percent removal is higher than when the adsorbent dosage is increased from 0.1 to 0.2 g. This indicates that with the adsorption, saturation of adsorption sites takes place, and hence with further increase in the adsorbent dosage from 0.2 to 0.4, the percentage of Fe removal remains almost constant. This may also result from aggregation by large adsorbates, reducing the adsorbent's active surface area [49].

## 4.4. Effect of temperature

The removal of iron ions by the adsorbent was observed to increase from 89.5 % at 25 °C to 93.2 % at 50 °C, and with further increase in temperature at 80 °C, the percentage of Fe removal was found to be 93.4 %, and equilibrium is almost established, as shown in Fig. 9. Higher diffusion rates and improved ion mobility at high temperatures may have

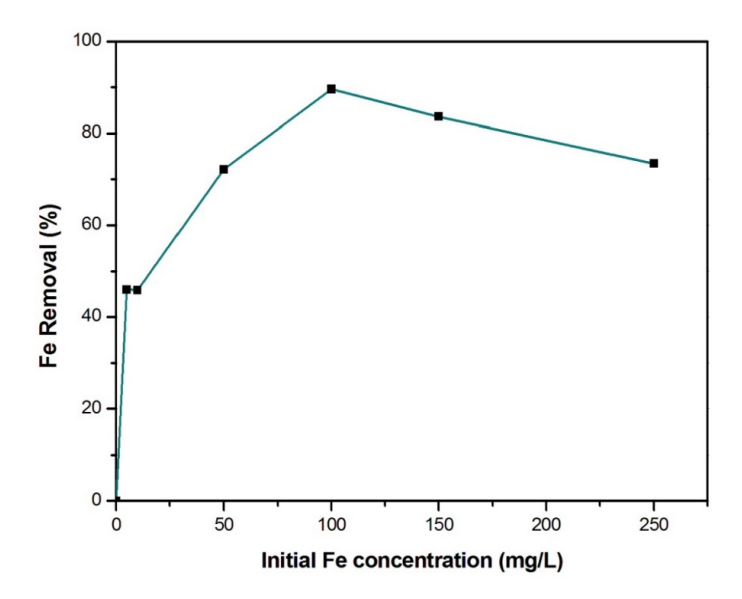


FIG. 7. Effect of initial metal ion (Fe) conc. on percentage removal of iron ions (adsorbent dosage, 0.1 g; contact time = 90 min.; 200 rpm agitation speed; room temperature)

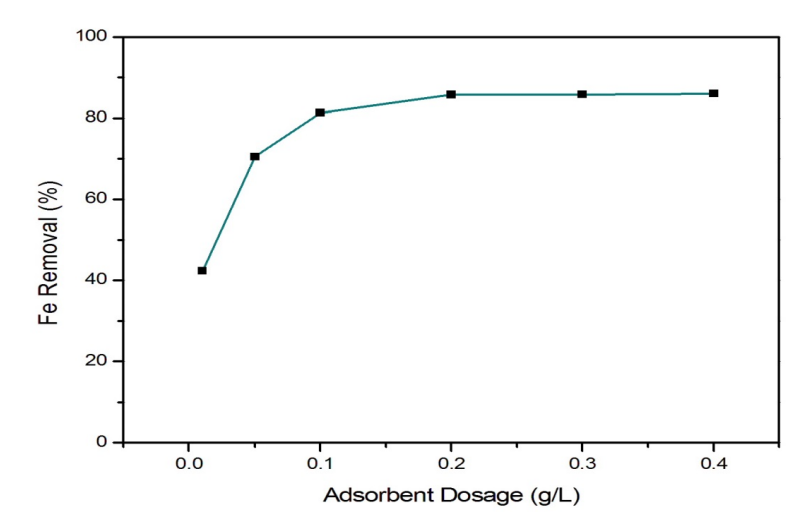


FIG. 8. Effect of adsorbent dose on percentage removal efficiency of iron (initial Fe conc. 100 mg/L; contact time = 90 min.; 200 rpm agitation speed; room temp.)

contributed to an increase in the percentage removal of iron ions [53]. Furthermore, the adsorbate's kinetic energy and surface activity increase with temperature [54].

#### 4.5. Adsorption isotherms

The removal of Fe ions by ZnSe:Ag:Urea nanoparticles at various initial Fe concentrations was examined using two fundamental adsorption isotherm models (Langmuir and Freundlich). The following are the equations for the Langmuir (3) and Freundlich (4) models [55]:

$$\frac{1}{q_e} = \frac{1}{q_0} + \frac{1}{q_0 K_L} \cdot \frac{1}{C_e},\tag{3}$$

$$\ln q_e = \ln K_f + \frac{1}{n} \ln C_e,\tag{4}$$

where  $q_e$  is the equilibrium adsorption capacity  $(\text{mg}\cdot\text{g}^{-1})$ ,  $q_m$  is the monolayer adsorption capacity  $(\text{mg}\cdot\text{g}^{-1})$ ,  $K_L$  is the Langmuir constant  $(\text{L}\cdot\text{mg}^{-1})$ ,  $K_F$  is the Freundlich constant  $(\text{L}\cdot\text{g}^{-1})$ , n is the Freundlich exponent and  $C_e$  is the concentration at equilibrium  $(\text{mg}\cdot\text{L}^{-1})$ . The adsorption isotherm provides information on the dependency of adsorption on the initial metal ion concentration and characterises the equilibrium of the adsorption material at the adsorbent surface. The Langmuir isotherm describes the monolayer adsorption onto a surface with homogenous adsorption sites, while the Freundlich model applies to multilayer adsorption on a heterogeneous surface (Fig. 11).

The Langmuir isotherm model (Fig. 10) has a higher correlation coefficient ( $R^2 = 0.976$ ) than the Freundlich isotherm model ( $R^2 = 0.958$ ). This result implies that the experimental data accords fairly well with the Langmuir

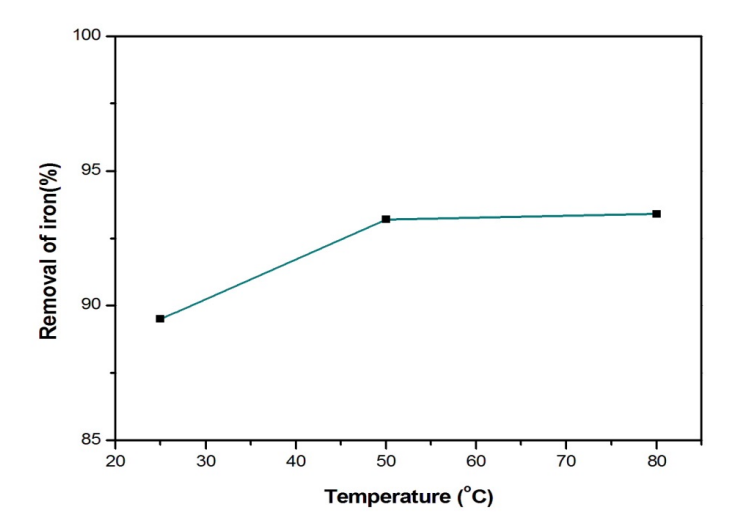


FIG. 9. Effect of temperature on percentage removal of iron (initial Fe conc.= 100 mg/L; contact time = 90 min.; 200 rpm agitation speed; adsorbent dosage = 0.2 g)

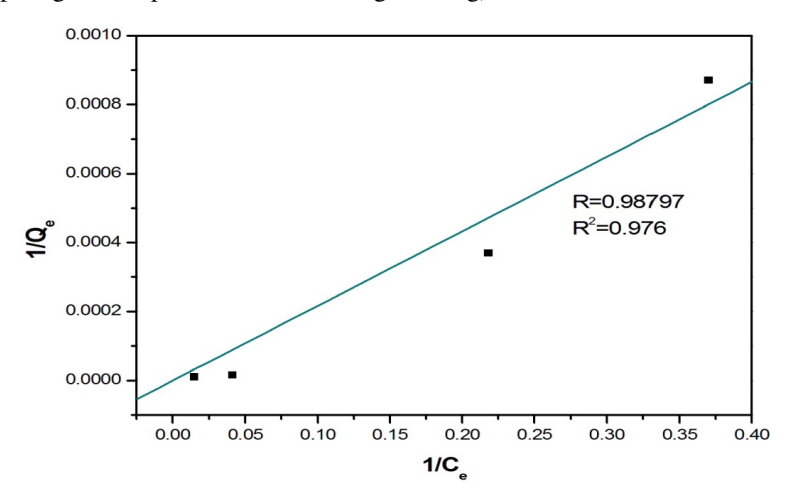


FIG. 10. Langmiur plot for adsorption of Fe on ZnSe:Ag:Urea

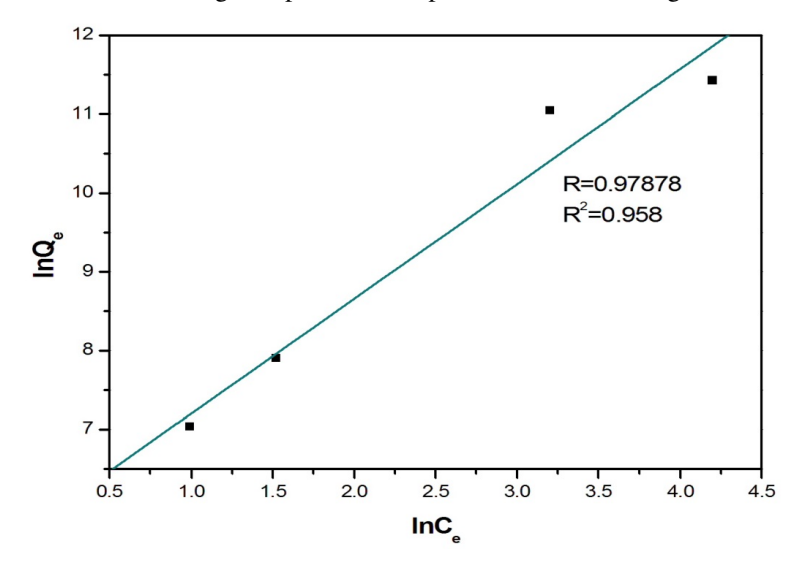


FIG. 11. Freundlich plot for adsorption of Fe on ZnSe:Ag:Urea

isotherm model. This indicates that the removal of Fe ions by ZnSe:Ag:Urea nanoparticles takes place through monolayer adsorption, with Fe ions homogeneously distributed on the adsorption sites on the adsorbent material surface.

#### 5. Conclusions

The present study reports the successful synthesis of nanostructured, urea and silver modified zinc selenide by a simple sol-gel method using hydrazine hydrate as a reducing agent and ethylene glycol as a stabilising agent, which prevents the agglomeration of synthesised nanoparticles. An investigation was conducted on their effectiveness as adsorbents to remove heavy metal iron ions from aqueous solutions. The physicochemical characterisation involved XRD, FE-SEM, EDX and FTIR spectroscopy. SEM images show spherical-like structures, which are more convenient for bactericidal and catalytic activation, evidencing the presence of N,C, O, Ag, Se and Zn. The XRD analysis gives the possible different phases and the diameter of the nanomaterial. The diameter of ZnSe:Ag:Urea was determined to be 19.911 nm. FTIR spectra confirm the new bond formation. Results from adsorption studies reveal that the equilibrium of the adsorption process was reached within a contact time of 80 minutes under room temperature. The increase in temperature increases the Fe removal percentage. Furthermore, with an increase in adsorbent dosage, the percentage removal of Fe first increases and eventually reaches an equilibrium state; however, with an increase in the initial iron concentration, the Fe removal percentage first increases and then decreases slightly until it reaches equilibrium. The maximum rate of Fe removal was found to be 89.5 % under the optimal room temperature conditions, with an adsorbent dosage of 0.1 g and an initial Fe concentration of 100 mg/L.

#### References

- [1] Tabassum H., Ahmad I.Z. Applications of metallic nanomaterials for the treatment of water. *Letters in Applied Microbiology, The Society for Applied Microbiology*, 2021, **75**, P. 731–743.
- [2] Shaikh R.B., Saifullah B., Rehman F.U. Greener Method for the Removal of Toxic Metal Ions from the Wastewater by Application of Agricultural Waste as an Adsorbent. *Water*, 2018, **10** (10).
- [3] Kolluru S.S., Agarwal S., Sireesha S., Sreedhar I., Kale S.R. Heavy metal removal from wastewater using nanomaterials-process and engineering aspects. *Process Safety and Environmental Protection*, 2021, **150**, P. 323–355.
- [4] Beena V., Rayar S.L., Ajitha S., Ahmad A., Albaqami M.D., Alsabar F.A.A., Sillanpää M. Synthesis and Characterization of Sr-Doped ZnSe Nanoparticles for Catalytic and Biological Activities. Water, 2021, 13, 2189.
- [5] Baby R., Hussein M.Z., Abdullah A.H., Zainal Z. Nanomaterials for the Treatment of Heavy Metal Contaminated Water. Polymers, 2022, 14, 583.
- [6] Silver J. Chemistry of Iron, first ed., Springer Science + Business Media, Dordrecht, 1993.
- [7] Green R., Charlton R., Seftel H., Bothwell T., Mayet F., Adams B., Finch C., Layrisse M. Body iron excretion in man: a collaborative study. *Am. J. Med.*, 1968, **45**, P. 336–353.
- [8] Khatri N., Tyagi S. Influences of natural and anthropogenic factors on surface and groundwater quality in rural and urban areas. *Front. Life Sci.*, 2015, **8**, P. 23–39.
- [9] Jusoh A.B., Cheng W.H., Low W.M., Nora'aini A., Noor M.J.M. Study on the removal of iron and manganese in groundwater by granular activated carbon. *Desalination*, 2005, **182**, P. 347–353.
- [10] Tekerlekopoulou A.G., Pavlou S., Vayenas D.V. Removal of ammonium, iron and manganese from potable water in biofiltration units: a review. *J. Chem. Technol. Biotechnol.*, 2013, **88**, P. 751–773.
- [11] Ellis D., Bouchard C., Lantagne G. Removal of iron and manganese from groundwater by oxidation and microfiltration. *Desalination*, 2000, 130, P. 255–264.
- [12] Sengupta A., Gupta A., Deb A.K. Arsenic crisis in Indian subcontinent: a local solution to a global problem. Water, 2001, 21, P. 34–36.
- [13] Kumar V., Bharti P.K., Talwar M., Tyagi A.K., Kumar P. Studies on high iron content in water resources of Moradabad district (UP), India. *Water Sci.*, 2017, **31** (1), P. 44–51.
- [14] Mahanta D.B., Das N.N., Dutta R.K. A chemical and bacteriological study of drinking water in tea gardens of central Assam. *Indian J. Environ. Prot.*, 2004, **24**, P. 654–660.
- [15] Sharma R., Shah S., Mahanta C. Hydrogeochemical study of groundwater fluoride contamination: a case study from Guwahati city India. *Asian J. Water Environ. Pollut.*, 2005, **2**, P. 47–54.
- [16] Houben G.J. Iron oxides in wells. Part 1. Genesis, mineralogy and geochemistry. Appl. Geochem., 2003, 18, P. 927–939.
- [17] World Health Organization. Iron in drinking water. In: *Guidelines for drinking-water quality*, 2nd ed. Vol. 2. Health criteria and other supporting information. World Health Organization, Geneva, 1996.
- [18] Khatri N., Tyagi S., Rawtani D. Assessment of drinking water quality and its health effects in rural areas of Harij Taluka, Patan district of Northern Gujarat. *Environ. Claims J.*, 2016, **28** (3), P. 223–246.
- [19] Zheng Q., Zhao Y., Guo J., Zhao S., Song L., Fei C., Zhang Z., Li X., Chang C. Iron overload promotes erythroid apoptosis through regulating HIF-1a/ROS signalling pathway in patients with myelodysplastic syndrome. *Leuk. Res.*, 2017, **58**, P. 55–62.
- [20] Hartmann J., Braulke F., Sinzig U., Wulf G., Maas J.H., Konietschke F., Haase D. Iron overload impairs proliferation of erythroid progenitors cells (BFU-E) from patients with myelodysplastic syndromes. *Leuk. Res.*, 2013, 37, P. 327–332.
- [21] Chai X., Li D., Cao X., Zhang Y., Mu J., Lu W., Xiao X., Li C., Meng J., Chen J., Li Q., Wang J., Meng A., Zhao M. ROS-mediated iron overload injures the hematopoiesis of bone marrow by damaging hematopoietic stem/progenitor cells in mice. *Sci. Rep.*, 2015, **5**, 10181.
- [22] Jang Y.Y., Sharkis S.J. A low level of reactive oxygen species selects for primitive hematopoietic stem cells that may reside in the low-oxygenic niche. *Blood*, 2007, **110**, P. 3056–3063.
- [23] Shao L., Li H., Pazhanisamy S.K., Meng A., Wang Y., Zhou D. Reactive oxygen species and hematopoietic stem cell senescence. *Int. J. Hematol.*, 2011. **94**. P. 24–32.
- [24] Frippiat C., Dewelle J., Remacle J., Toussaint O. Signal transduction in H<sub>2</sub>O<sub>2</sub>-induced senescence-like phenotype in human diploid fibroblasts. *Free Radic. Biol. Med.*, 2002, **33**, P. 1334–1346.
- [25] Prus E., Fibach E. Effect of iron chelators on labile iron and oxidative status of thalassaemic erythroid cells. Acta Haematol., 2010, 123, P. 14–20.

- [26] Alimohammadi V., Sedighi M., Jabbari E. Experimental study on efficient removal of total iron from wastewater using magnetic-modified multi-walled carbon nanotubes. Ecol. Eng., 2017, 102, P. 90–97.
- [27] Das B., Hazarika P., Saikia G., Kalita H., Goswami D.C., Das H.B., Dube S.N., Dutta R.K. Removal of iron by groundwater by ash: a systematic study of a traditional method. *J. Hazard. Mater.*, 2007, **141**, P. 834–841.
- [28] Michalakos G.D., Nieva J.M., Vayenas D.V., Lyberatos G. Removal of iron from potable water using a Trickling filter. *Wat. Res.*, 1997, **31** (5), P. 991–996.
- [29] Shalini chaturvedi. Removal of iron for safe drinking water. Desalination, 2012, URL: https://www.academia.edu/125112372/Removal\_of\_iron\_for\_safe\_drinking\_water.
- [30] Helal E.H.D., Dessouki H.A., Nassar M.Y., Ahmed I.S. Preparation and spectral analysis of nanosized ZnSe particles. *J. Basic Environ. Sci.*, 2018, 5, P. 20–24.
- [31] Dehghani S., et al. Zinc selenide nanoparticles: Green synthesis and biomedical applications. Nanomed. J., 2022, 9, P. 15–23.
- [32] Yang Y., Wu Z., Yang R., Li Y., Liu X., Zhang L., Yu B. Insights into the mechanism of enhanced photocatalytic dye degradation and antibacterial activity over ternary ZnO/ZnSe/MoSe<sub>2</sub> photocatalysts under visible light irradiation. *Appl. Surf. Sci.*, 2021, **539**, 148220.
- [33] Beena V., Ajitha S., Rayar S.L., Parvathiraja C., Kannan K., Palani G. Enhanced Photocatalytic and Antibacterial Activities of ZnSe Nanoparticles. *J. Inorg. Organomet. Polym. Mater.*, 2021, **4**, P. 1–12.
- [34] Archana J., Mani S., M N., Ponnusamy S., Muthamizhchelvan C., Hayakawa Y. Chemical synthesis and functional properties of hexamethylenete-tramine capped ZnSe nanorods. *Mater Lett.*, 2014, **125**, P. 32–35.
- [35] Yang J., Wang G., Liu H., Park J., Gou X., Cheng X. Solvothermal synthesis and characterization of ZnSe nanoplates. J Cryst Growth., 2008, 310, P. 3645–3648.
- [36] Lei Z., Wei X., Bi S., He R. Reverse micelle synthesis and characterization of ZnSe nanoparticles. Mater. Lett., 2008, 62, P. 3694–3696.
- [37] Hao H., Yao X., Wang M. Preparation and optical characteristics of ZnSe nanocrystals doped glass by sol-gel in situ crystallization method. Opt. Mater., 2007, 29, P. 573–577.
- [38] Panneerselvam A., Malik A., O'Brien P., Nguyen C.Q. The CVD of silver selenide films from dichalcogenophosphinato and imidodichalcogenodiphosphinatosilver(I) single-source precursors. *J. of Materials Chemistry*, 2009, **19** (3).
- [39] Sharma P. Synthesis and characterization of Ag-chalcogenide nanoparticles for possible applications in photovoltaics. *Materials Science Poland*, 2018, **36** (3), P. 375–380.
- [40] Thendral M., et al. Nucleation and spectroscopic studies of manganese doped new nlo organic crystal. *Int. J. of Current Research in Life Sciences*, 2018, 7 (5), P. 2121–2125.
- [41] Madhurambal G., Mariappan M. Growth and characterization of urea-thiourea non-linear optical organic mixed crystal. *Indian J. of Pure & Applied Physics*, 2010, **48**, P. 264–270.
- [42] Shameli K., et al. Green biosynthesis of silver nanoparticles using Curcuma longa tuber powder. Int. J. of Nanomedicine, 2012, P. 5603–5610.
- [43] Manivannan M., et al. Investigation of inhibitive action of urea-Zn2+ system in the corrosion control of carbon steel in sea water. *Int. J. of Engineering Science and Technology*, 2011, **3** (11), P. 8048–8060.
- [44] Ahamed A.J., et al. Synthesis and Characterization of ZnSe Nanoparticles by Co-precipitation Method. J. of Nanoscience and Technology, 2016, 2, P. 148–150.
- [45] Penland R.B., Mizushima S., Curran C., Quagliano J.V. Infrared Absorption Spectra of Inorganic Coördination Complexes. X. Studies of Some Metal-Urea Complexes. J. of the American Chemical Society, 1957, 79 (7), P. 1575–1578.
- [46] Jackovitz J.F., Walter J.L. Infrared absorption spectra of metal-amino acid complexes–V. The infrared spectra and normal vibrations of metal-leucine chelates. *Spectrochimica Acta*, 1966, **22** (8), P. 1393–1406.
- [47] Megahed A.S., Ibrahim O.B., Adam A.M.A., AL-Majthoub M.M. The Chelating Behavior of Urea Complexed with the Metal Ions of Copper (II), Zinc (II), Silver (I), Cadmium (II) and Mercury (II) at Room Temperature. *Research J. of Pharmaceutical, Biological and Chemical Sciences*, 2014, 5 (2), P. 970–980.
- [48] Nakamoto K. Infrared and Raman spectra of inorganic and coordination compounds, part B: applications in coordination, organometallic, and bioinorganic chemistry. John Wiley & Sons, 2009.
- [49] Kakavandi B., Esrafili A., Mohseni-Bandpi A., Jafari A.J., Kalantary R.R. Magnetic Fe<sub>3</sub>O<sub>4</sub>@C nanoparticles as adsorbents for removal of amoxicillin from aqueous solution. *Water Sci. Technol.*, 2014, **69** (1), P. 147–155.
- [50] Arbanah M., Najwa M.R.M., Halim K.H.K. Biosorption of Cr (III), Fe (II), Cu (II), Zn (II) ions from liquid laboratory chemical waste by Pleurotus ostreatus. *Int. J. Biotechnol. Wellness Ind.*, 2012, P. 152–162.
- [51] Luo C., Tian Z., Yang B., Zhang L., Yan S. Manganese dioxide/iron oxide/acid oxidized multi-walled carbon nanotube magnetic nanocomposite for enhanced hexavalent chromium removal. *Chem. Eng. J.*, 2013, **234**, P. 256–265.
- [52] Jung C., Heo J., Han J., Her N., Lee S.-J., Oh J., Ryu J., Yoon Y. Hexavalent chromium removal by various adsorbents: powdered activated carbon, chitosan, and single/multi-walled carbon nanotubes. *Sep. Purif. Technol.*, 2013, **106**, P. 63–71.
- [53] Kaveeshwar A.R., Sanders M., Ponnusamy S.K., Depan D. et al. Chitosan as a biosorbent for adsorption of iron (II) from fracking wastewater. *Polym. Adv. Technol.*, 2018, **29**, P. 961–969.
- [54] Jain C.K., Malik D.S., Yadav A.K. Applicability of plant based biosorbents in the removal of heavy metals: A review. Environ. Process, 2016, 3, P. 495–523.
- [55] Li J., Fan M.J., Li M., Liu X. Cr(VI) removal from groundwater using double surfactant-modified nanoscale zero-valent iron (nZVI): Effects of materials in different status. Sci. Total Environ., 2020, 717, 137112.

Information about the authors:

*Khurshed A. Shah* – PG Department of Physics, Sri Pratap College, Cluster University Srinagar, J&K-190001, India; ORCID 0000-0002-2694-4515; drkhursheda@gmail.com

*Humaira S. Wani* – Department of Applied Sciences, Institute of Technology, Zakura Campus, University of Kashmir, Srinagar, J&K-190006, India; ORCID 0009-0003-1238-9412; wanihumaira1@gmail.com

S. M. A. Andrabi – Department of Applied Sciences, Institute of Technology, Zakura Campus, University of Kashmir, Srinagar, J&K-190006, India; ORCID 0009-0001-7331-1358; muzaffar2000@gmail.com

*Quinton L. Williams* – Department of Physics and Astronomy, Howard University, 2355 6th St., NW, Washington, DC 20059, USA; ORCID 0000-0002-9244-6661; quinton.williams@howard.edu

Data availability statement: The datasets generated or analysed during the current study are available from the corresponding author upon reasonable request.

*Conflict of interest*: The authors declare that they have no known competing financial interests or personal relationships that could have appeared to influence the work reported in this paper.